Supporting information

Intramolecular charge transfer effect for highly efficient deep red and near infrared thermally activated delayed fluorescence

Chen-Zong Yang,†[a] Ze-Hui Pan,†[a] Kai Zhang,†[b] Jing-Wen Tai,[a] Chuan-Kui Wang,*[b] Lei Ding,*[c] Man-Keung Fung*[a] and Jian Fan*[ad]

[a] Institute of Functional Nano & Soft Materials (FUNSOM), Jiangsu Key Laboratory for Carbon-Based Functional Materials & Devices, Soochow University, Suzhou, Jiangsu 215123, China

[b] Shandong Province Key Laboratory of Medical Physics and Image Processing Technology, School of Physics and Electronics, Shandong Normal University, 250014 Jinan, China.

[c] School of Chemistry and Life Sciences, Suzhou University of Science and Technology, Suzhou, Jiangsu 215009, China

[d] State Key Laboratory of Structural Chemistry, Fujian Institute of Research on Structure of Matter, Chinese Academy of Sciences, Fuzhou, Fujian 35002, China

E-mail: ckwang@sdnu.edu.cn, dinglei@usts.edu.cn, mkfung@suda.edu.cn, jianfan@suda.edu.cn

†These authors contribute equally to this work.

1. General Information

All reactions were performed under nitrogen atmosphere unless otherwise stated. Dry toluene (Tol) were purified by PURE SOLV (Innovative Technology) purification system. ^{1}H NMR and ^{13}C NMR spectra were recorded on a Bruker 400 MHz and Agilent DD2-600 MHz NMR spectrometer at ambient temperature. Matrix-Assisted Laser Desorption/Ionization Time of Flight Mass Spectrometry (MALDI-TOF-MS) was measured with a Bruker ultraflextreme MALDI-TOF spectrometer. UV-vis absorption spectra were recorded on Cary 60 spectrometer (Agilent Technologies). PL spectra and phosphorescent spectra were recorded on a Hitachi F-4600 fluorescence spectrophotometer. Differential scanning calorimetry (DSC) was performed on a TA DSC 2010 unit at a heating rate of 10 ^{o}C min^{-1} under nitrogen. The glass transition temperatures (T_g) were determined from the second heating scan. Thermogravimetric analysis (TGA) was performed on a TA SDT 2960 instrument at a heating rate of 10 ^{o}C min^{-1} under nitrogen. Temperature at 5% weight loss was used as the decomposition temperature (T_d). Cyclic voltammetry (CV) was carried out on a CHI600 voltammetric analyzer at room temperature with ferrocenium-ferrocene (Fc$^+$/Fc) as the external standard. The oxidative scans were performed using 0.1 M n-Bu$_4$NPF$_6$ (TBAPF$_6$) in deoxygenated dichloromethane as the supporting electrolyte. A conventional three-electrode configuration consisting of a Pt-wire counter electrode, an Ag/AgCl reference electrode, and a Glassy-Carbon working electrode was used. The cyclic voltammograms were obtained at a scan rate of 0.1 V s^{-1}. All the calculations were carried out in Gaussian 16 package.[1]

2. OLED fabrication and characterization

Devices were fabricated on patterned ITO glass substrates with a sheet resistance of 15 Ω per square. Before device fabrication, ITO substrates were ultrasonically cleaned sequentially with acetone, ethanol, and deionized water, dried in an oven at 100 °C for 3 h, then treated with UV-ozone for 15 min, and finally loaded into a deposition chamber with a basic pressure of 4×10^{-6} Torr. Deposition rates and thicknesses of all materials were monitored with oscillating quartz crystals. The deposited rates for organic materials, Liq, and Al were controlled at 2-3, 0.2, and 4-6Å s^{-1}, respectively. The current-voltage characteristics were measured with a computer-controlled Keitheley 2400 source meter. Electroluminescence spectra were measured with a PHOTO RESEARCH SpectraScan PR 745 PHOTOMETER, which can detect in the

spectral region 380-1080 nm. All the measurements were carried out under ambient atmosphere at room temperature.

The EQE of the emission was obtained by measuring the light intensity in the forward direction and assuming the external emission profile to be Lambertian. Therefore, the EQE can be calculated using the following equations.[2]
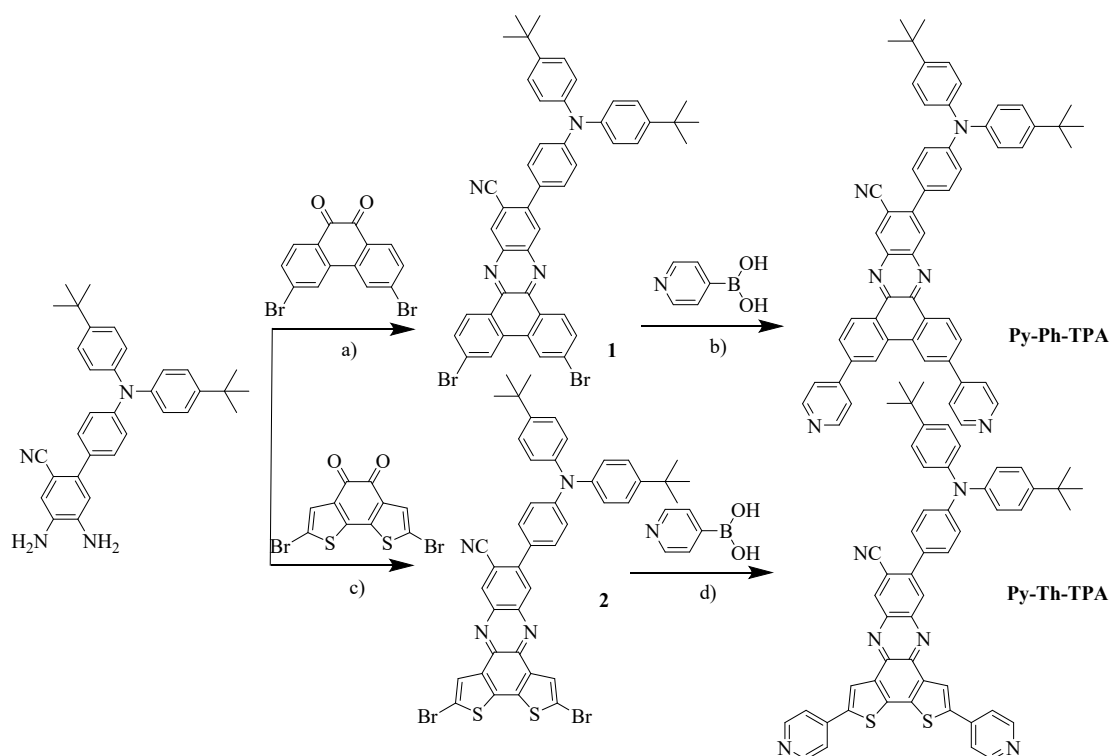
$$EQE = \frac{N_P}{N_E}$$

$$N_P = \frac{\int L_E(\lambda) \cdot W(\lambda) \cdot d\lambda}{h \times c} \times \pi \times D$$

$$N_E = \frac{I}{e}$$

Where N_E is the number of electrons, N_P is the number of photons, $L_E(\lambda)$ is spectral radiance (W sr^{-1} m^{-2} nm^{-1}), $W(\lambda)$ is wavelength, $d\lambda = 2$, D is emitting area, h is Planck's constant, e is the charge of an electron, c is the speed of light in vacuum and I is the current injected.

3. Synthetic procedure and characterization

Scheme S1. Synthetic procedure of **Py-Ph-TPA, Py-Th-TPA:** a)/c) AcOH, 125 °C, overnight; b) Pd(PPh$_3$)$_4$, K$_2$CO$_3$, toluene/CH$_3$CH$_2$OH/H$_2$O, 110 °C, 36 h; d) Pd(PPh$_3$)$_4$, K$_2$CO$_3$, THF/CH$_3$CH$_2$OH/H$_2$O, 70 °C, 12 h.

12-(4-(bis(4-(tert-butyl)phenyl)amino)phenyl)-3,6-dibromodibenzo[a,c]phenazine-11-carbonitrile (1)

4,5-diamino-4'-(bis(4-(tert-butyl)phenyl)amino)-[1,1'-biphenyl]-2-carbonitrile (1.2 g, 2.46 mmol) and 3,6-dibromophenanthrene-9,10-dione (900 mg, 2.46 mmol) was suspended in AcOH (120 mL) and heated at 125 °C overnight under nitrogen. After cooling to room temperature, the solution was poured into ice water. The separated solid was filtered off and washed with water, and then dried under vacuum. The crude product was re-crystallized in EtOH to afford compound **1** (1.47 g, 73.4%). ^{1}H NMR (400 MHz, CDCl$_3$) δ 9.20 (d, J = 8.4 Hz, 2H), 8.76 (s, 1H), 8.59 (s, 2H), 8.36 (s, 1H), 7.89 (d, J = 4.5 Hz, 2H), 7.61 (d, J = 7.6 Hz, 2H), 7.34 (d, J = 7.5 Hz, 4H), 7.17 (dd, J = 17.7, 7.4 Hz, 6H), 1.34 (s, 18H). MALDI-TOF-MS: m/z calcd for C$_{47}$H$_{38}$Br$_2$N$_4$: 818.146, found: 818.427.

10-(4-(bis(4-(tert-butyl)phenyl)amino)phenyl)-2,5-dibromodithieno[3,2-a:2',3'-c]phenazine-9-carbonitrile (2)

4,5-diamino-4'-(bis(4-(tert-butyl)phenyl)amino)-[1,1'-biphenyl]-2-carbonitrile (800 mg, 1.64 mmol) and 2,7-dibromobenzo[2,1-b:3,4-b']dithiophene-4,5-dione (619 mg, 1.64 mmol) was suspended in AcOH (120 mL) and heated at 125 °C overnight under nitrogen. After cooling to room temperature, the solution was poured into ice water. The separated solid was filtered off and washed with water, and then dried under vacuum. The crude product was re-crystallized in EtOH to afford compound **2** (853 mg, 62.7%). ^{1}H NMR (400 MHz, CDCl$_3$) δ 8.77 (s, 1H), 8.40 (t, J = 5.6 Hz, 2H), 8.35 (s, 1H), 7.61 (d, J = 8.7 Hz, 2H), 7.33 (d, J = 8.7 Hz, 4H), 7.16 (dd, J = 15.5, 8.7 Hz, 6H), 1.34 (s, 18H). MALDI-TOF-MS: m/z calcd for C$_{43}$H$_{34}$Br$_2$N$_4$S$_2$: 830.059, found: 829.999.

12-(4-(bis(4-(tert-butyl)phenyl)amino)phenyl)-3,6-di(pyridin-4-yl)dibenzo[a,c]phenazine-11-carbonitrile (Py-Ph-TPA)

Compound **1** (800 mg, 0.98 mmol), pyridin-4-ylboronic acid (360 mg, 2.93 mmol), K$_2$CO$_3$ (271 mg, 1.96 mmol) and Pd(PPh$_3$)$_4$ (57 mg, 0.049 mmol) were added to 100 mL mixture of toluene, ethanol and water (100/10/1, v/v/v). The reaction system was stirred and refluxed under nitrogen for 36 h. After cooling to room temperature, the solvent was removed under reduced pressure, and then the reaction mixture was extracted with dichloromethane and water. After removal of the solvent, the residue was purified by column chromatography with DCM/Et$_3$N (5:1, v/v) to afford the compound Py-Ph-TPA (523 mg, 65.5%). ^{1}H NMR (600 MHz, CDCl$_3$) δ 9.48 (t, J = 7.9

Hz, 2H), 8.81 (t, J = 8.5 Hz, 7H), 8.40 (s, 1H), 8.11-7.96 (m, 2H), 7.75 (d, J = 4.6 Hz, 4H), 7.63 (d, J = 8.5 Hz, 2H), 7.34 (d, J = 8.4 Hz, 4H), 7.20 (d, J = 8.4 Hz, 2H), 7.15 (d, J = 8.5 Hz, 4H), 1.35 (s, 18H). ^{13}C NMR (101 MHz, CDCl$_3$) δ 179.55, 150.76, 150.62, 149.37, 147.72, 146.84, 146.62, 145.95, 144.33, 144.27, 143.51, 143.47, 143.02, 141.19, 140.87, 139.89, 139.07, 137.40, 135.99, 133.45, 132.74, 132.27, 131.63, 131.10, 130.38, 130.29, 129.80, 129.45, 128.92, 128.65, 127.94, 127.67, 127.35, 127.27, 126.35, 125.07, 122.75, 122.02, 121.73, 121.06, 118.35, 113.62, 34.42, 31.46. MALDI-TOF-MS: m/z calcd for C$_{57}$H$_{46}$N$_6$: 814.378, found: 814.431.

10-(4-(bis(4-(tert-butyl)phenyl)amino)phenyl)-2,5-di(pyridin-4-yl)dithieno[3,2-a:2',3'-c]phenazine-9-carbonitrile (Py-Th-TPA)

Compound **2** (800 mg, 0.96 mmol), pyridin-4-ylboronic acid (356 mg, 2.89 mmol), K$_2$CO$_3$ (260 mg, 1.92 mmol) and Pd(PPh$_3$)$_4$ (55 mg, 0.048 mmol) were added to 100 mL mixture of THF, ethanol and water (100/10/1, v/v/v). The reaction system was stirred and refluxed under nitrogen for 12 h. After cooling to room temperature, the solvent was removed under reduced pressure, and then the reaction mixture was extracted with dichloromethane and water. After removal of the solvent, the residue was purified by column chromatography with DCM/Et$_3$N (5:1, v/v) to afford the compound Py-Th-TPA (423 mg, 53.3%). ^{1}H NMR (400 MHz, CDCl$_3$) δ 8.81 (d, J = 9.4 Hz, 3H), 8.74 (s, 4H), 8.39 (s, 1H), 7.71 (s, 4H), 7.62 (d, J = 6.9 Hz, 2H), 7.35 (d, J = 7.9 Hz, 4H), 7.22-7.10 (m, 6H), 1.35 (s, 18H). MALDI-TOF-MS: m/z calcd for C$_{53}$H$_{42}$N$_6$S$_2$: 826.291, found: 826.318.
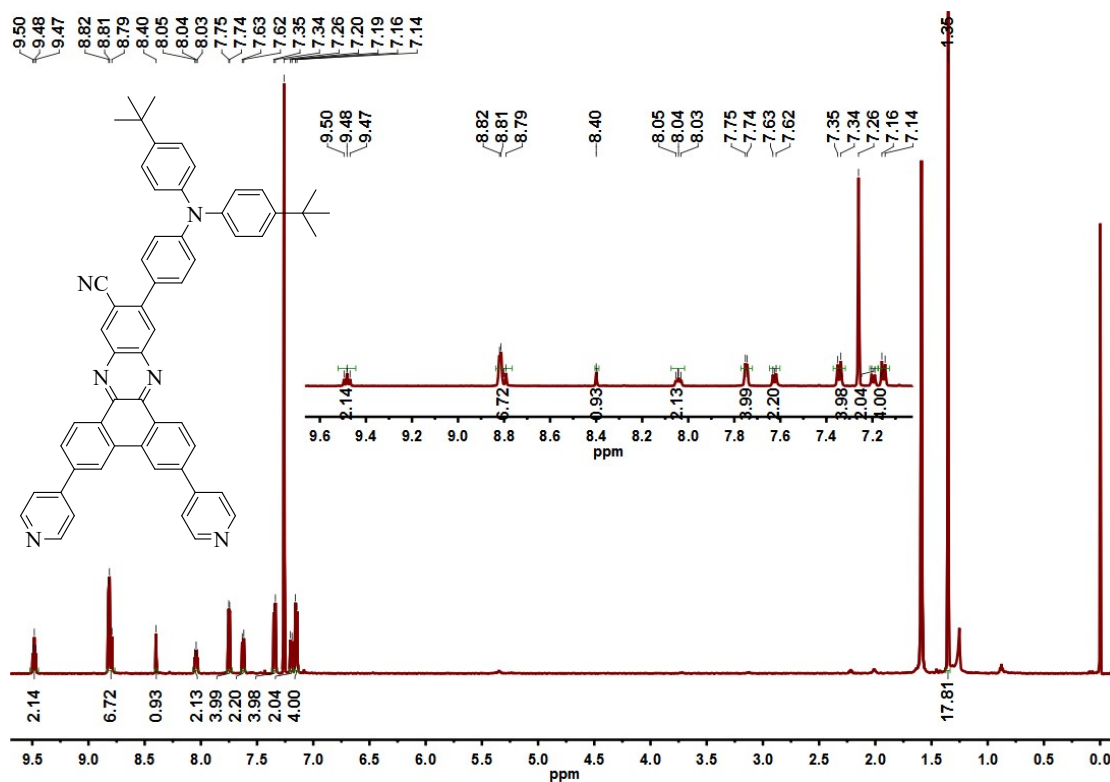
Figure S1. ^{1}H NMR spectrum (CDCl$_3$, 600 MHz) of Py-Ph-TPA.
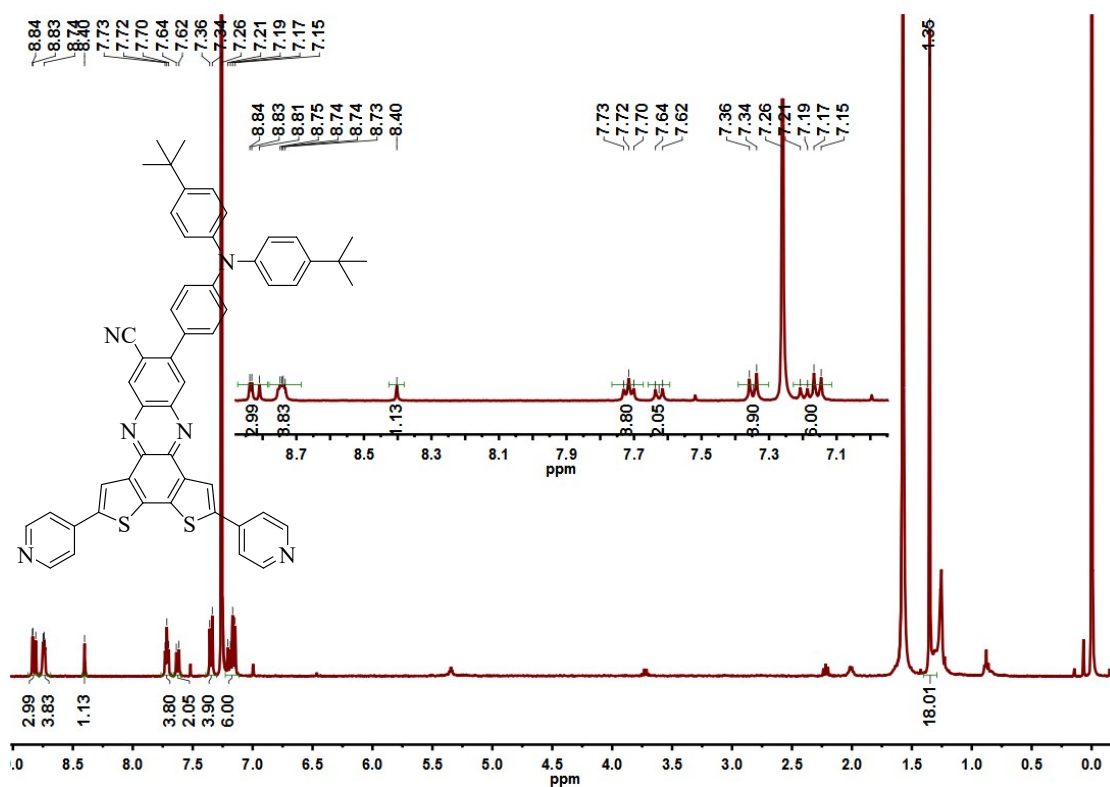
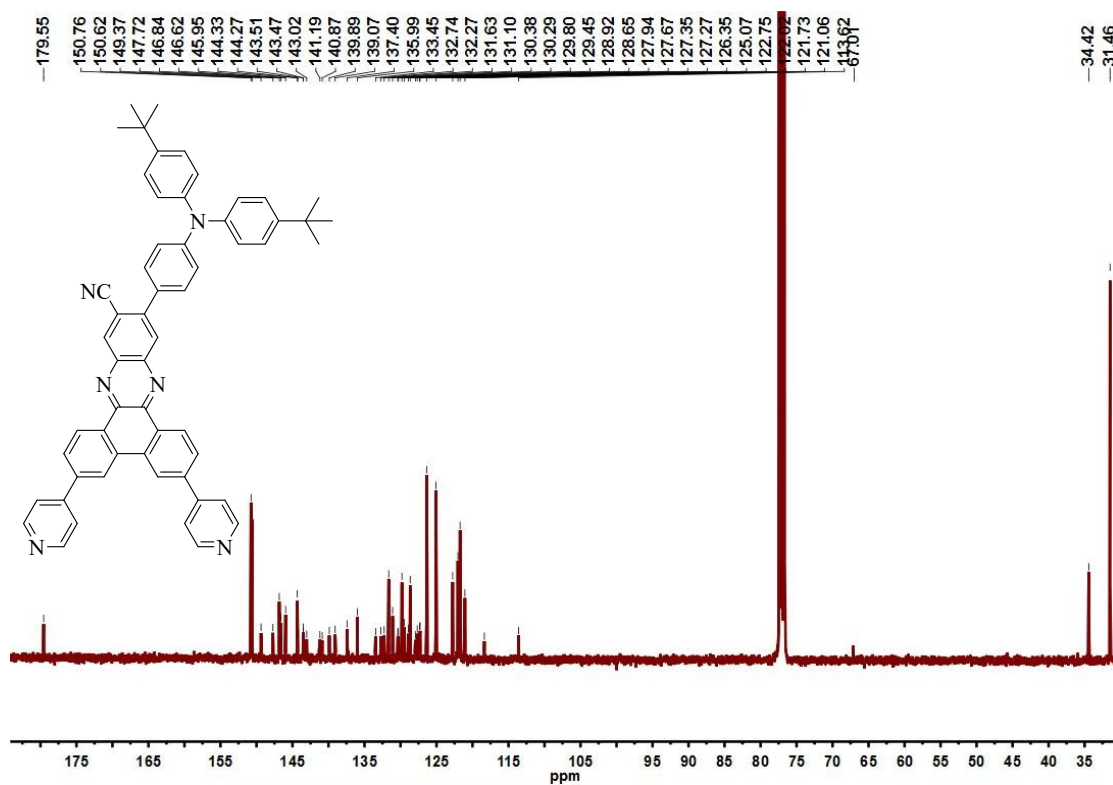**Figure S2.** ^{1}H NMR spectrum (CDCl$_3$, 400 MHz) of Py-Th-TPA.

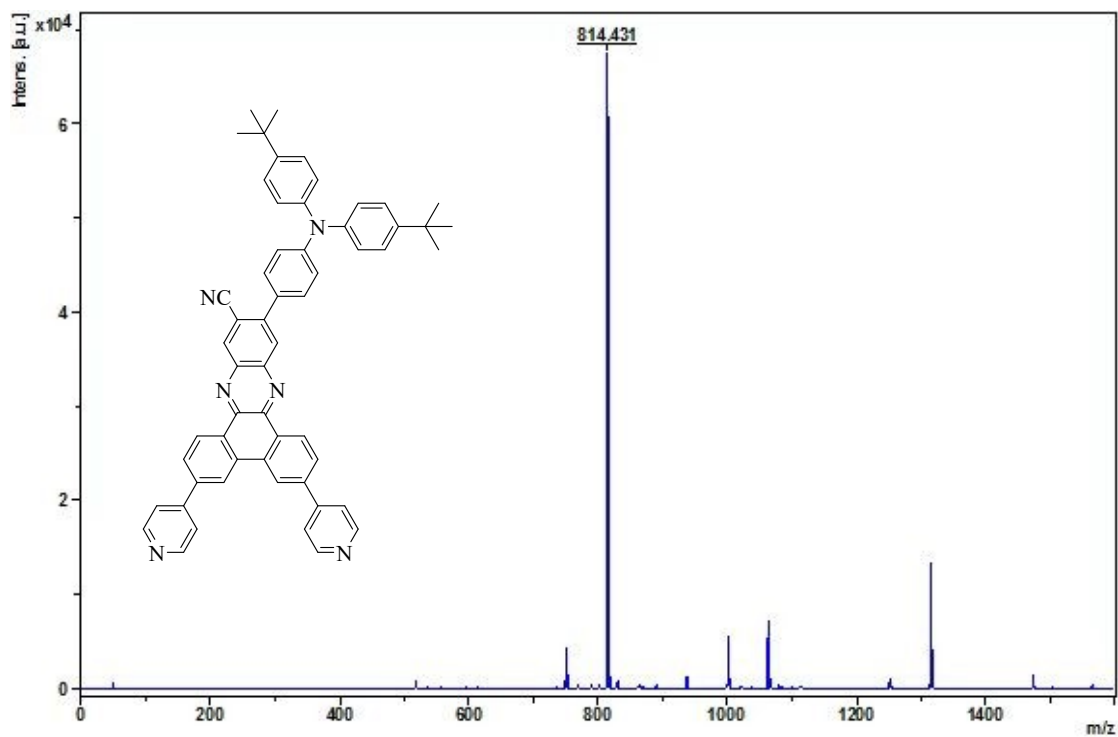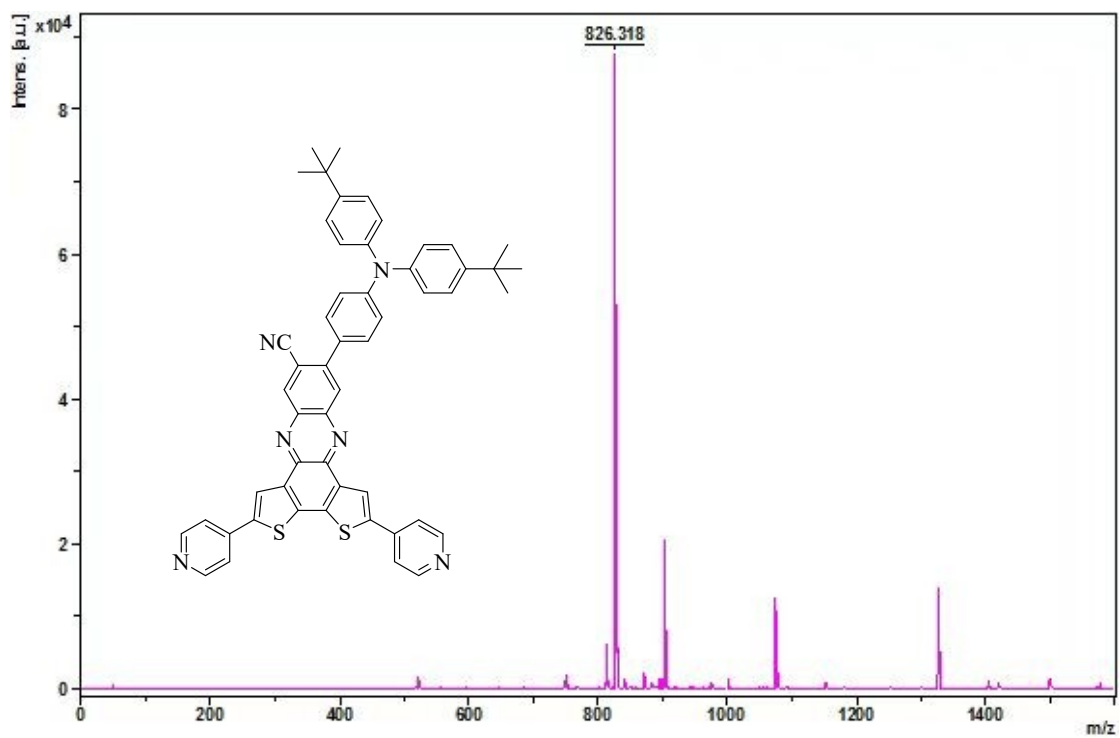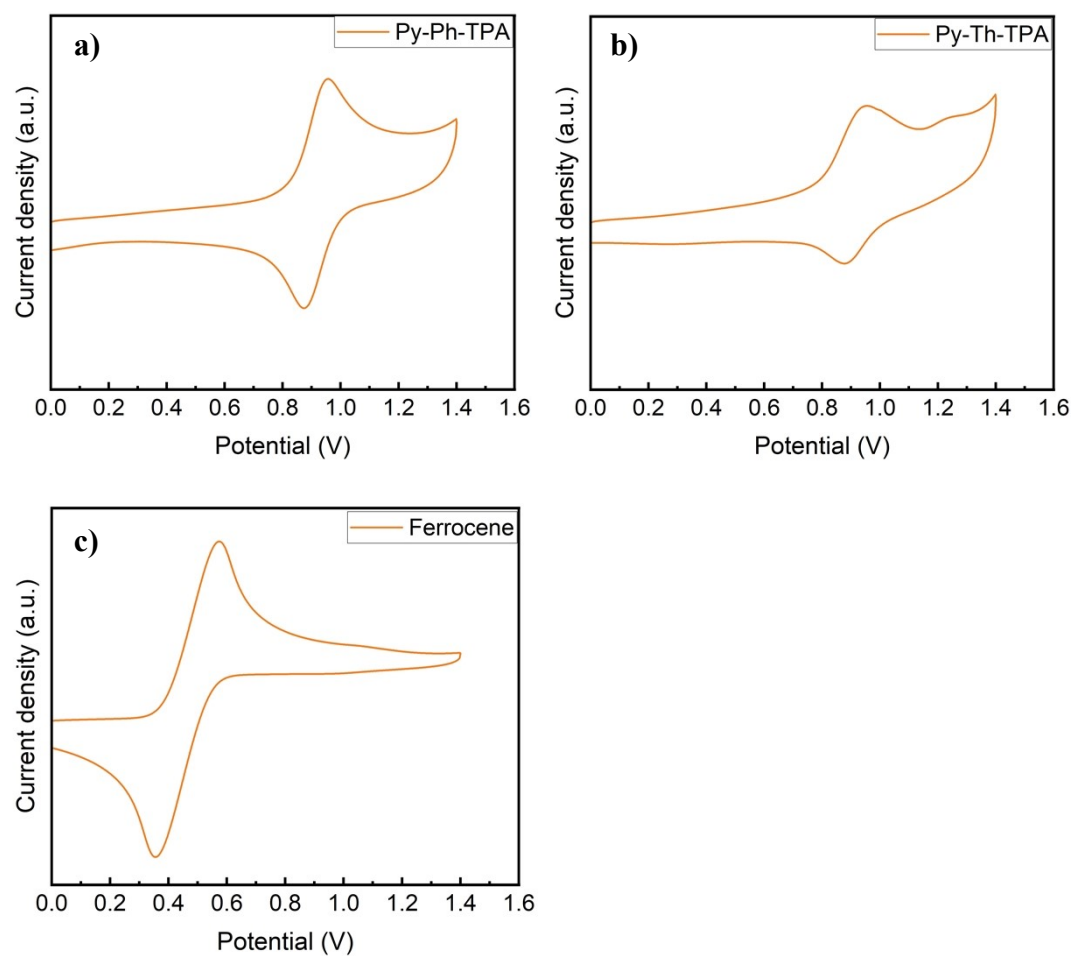**Figure S3.** ^{13}C NMR spectrum (CDCl$_3$, 101 MHz) of Py-Ph-TPA.
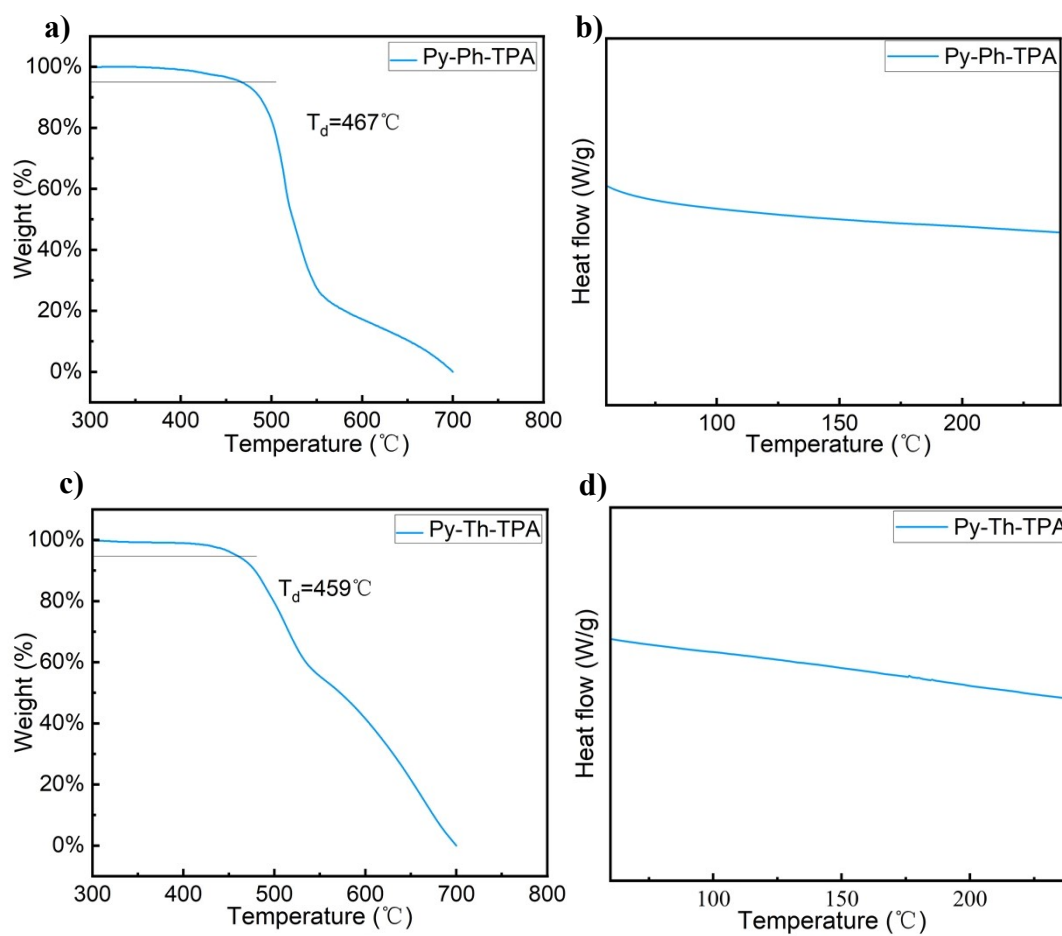

Figure S4. MALDI-TOF mass spectrum of Py-Ph-TPA.

Figure S5. MALDI-TOF mass spectrum of Py-Th-TPA.

4. Electrochemical and thermal and properties

Figure S6. Cyclic voltammograms of Py-Ph-TPA, Py-Th-TPA and Ferrocene.
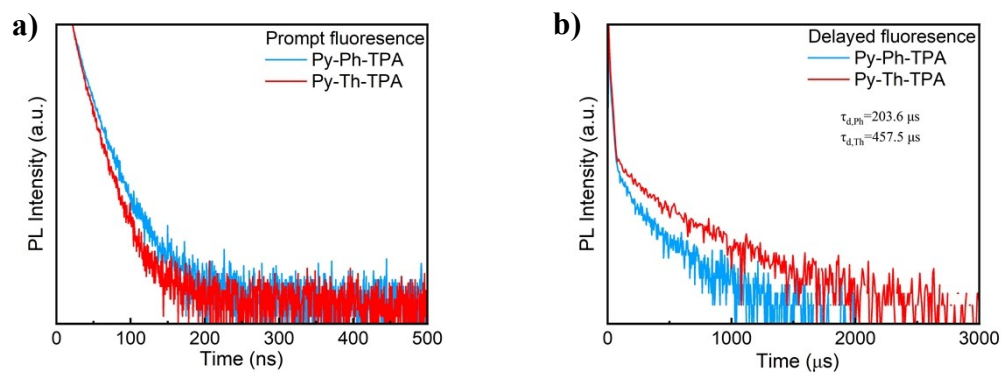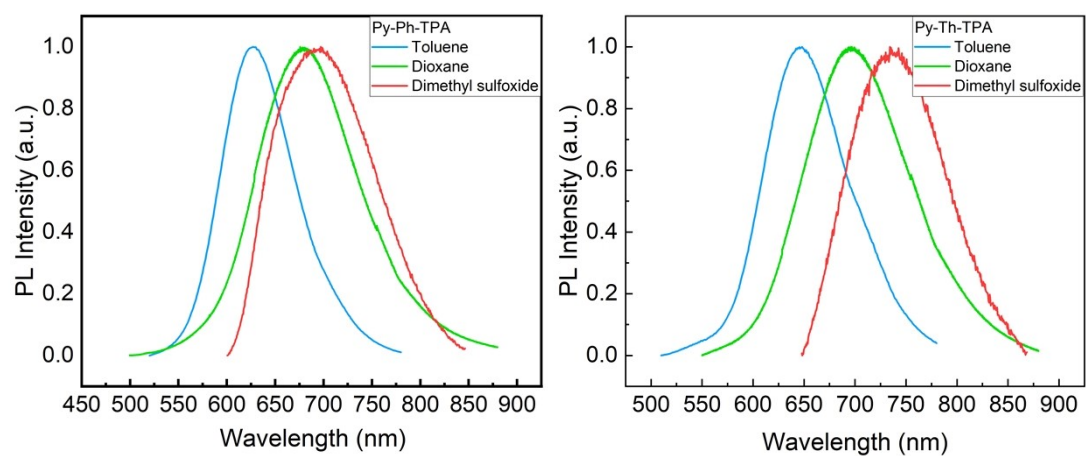
Figure S7. TGA (left) and DSC (right) curves of Py-Ph-TPA and Py-Th-TPA at a heating rate of 10 °C/min under N_2.

5. Photophysical properties

Figure S8. Transient PL decay curves of Py-Ph-TPA and Py-Th-TPA in 5 wt% doped CBP film.

Figure S9. Normalized PL spectra of Py-Ph-TPA and Py-Th-TPA in various solutions with different polarities.

6. Calculation formulas for the photophysical parameters

Ignoring singlet internal conversion (IC) process, the main rate constants were determined by using the following equations:Ignoring singlet internal conversion (IC) process, the main rate constants were determined by using the following equations:

$$k_p = \frac{1}{\tau_p}$$

$$k_d = \frac{\Phi_d}{\tau_d \Phi_{ISC}}$$

$$k_r^S = \Phi_p \cdot k_p$$

$$k_{ISC} = k_p - k_r^S$$

$$k_{RISC} = \frac{k_p \cdot k_d \Phi_d}{k_{ISC} \ \Phi_p}$$

$$k_{nr}^T = k_d - \left(1 - \frac{k_{ISC}}{k_r^S + k_{ISC}}\right) \cdot k_{RISC}$$

$$\Phi_{ISC} = 1 - \Phi_p$$

Φ_{PL} is the absolute photoluminescence quantum yield; Φ_p is the prompt fluorescent component of Φ_{PL}; Φ_d is the delayed fluorescent component of Φ_{PL}; τ_p is the lifetime of prompt fluorescent; τ_d is the lifetime of delayed fluorescent; k_p is the rate constant of prompt fluorescence decay; k_d is the rate constant of delayed fluorescence decay; k_r^S is the rate constant of radiative transition from S_1 to S_0; k_{ISC} is the rate constant of intersystem crossing; k_{RISC} is the rate constant of reverse intersystem crossing; k_{nr}^T is the non-radiative decay rate constant from T_1 to S_0; Φ_{ISC} is the quantum efficiency of intersystem crossing process.

Table S1. Photophysical characteristics of Py-Ph-TPA and Py-Th-TPA in CBP (5 wt% doped film).

Compound	Φ_{PL} [%]	Φ_p/Φ_d [%]	τ_p [ns]	τ_d [μs]	k_p [10^7 s^{-1}]	k_d [10^3 s^{-1}]	k_r^S [10^7 s^{-1}]	k_{ISC} [10^7 s^{-1}]	k_{RISC} [10^3 s^{-1}]	k_{nr}^T [10^2 s^{-1}]
Py-Ph-TPA	100	31.7/68.3	14.9	203.6	6.7	4.9	2.1	4.6	15	0
Py-Th-TPA	71	37.6/33.4	11.1	457.5	9.0	1.2	3.4	5.6	1.7	5.5

Table S2. Summary of EL performance for the devices based on Py-Ph-TPA and Py-Th-TPA in CBP.

Emitter	Dopant ratio	V_{on}[a] (V)	L_{max}[b] (cd/m^2)	CE[c] (cd/A^1)	PE[d] (lm/W^1)	λ_{max}[e] (nm)	EQE[f] (%)	CIE[g] (x, y)
Py-Ph-TPA	3%	2.5	2764	32.48	43.84	632	31.06	(0.63, 0.36)
	5%	2.5	3788	24.42	34.87	648	32.48	(0.65, 0.34)
	7%	2.5	1576	14.11	18.47	656	25.80	(0.66, 0.33)
	10%	2.5	3648	9.14	13.06	666	24.22	(0.67, 0.32)
	15%	2.5	2852	4.80	6.85	680	18.72	(0.68, 0.31)
	25%	2.5	1754	2.38	3.04	688	13.10	(0.69, 0.30)
Py-Th-TPA	3%	2.7	946.6	7.89	10.32	652	13.62	(0.64, 0.35)
	5%	2.7	1046	6.89	9.40	660	15.48	(0.66, 0.33)
	7%	2.7	830.6	5.58	7.62	674	20.25	(0.67, 0.32)
	10%	2.7	642.3	3.93	5.37	690	17.59	(0.68, 0.32)
	15%	2.8	476.6	0.94	1.23	706	11.30	(0.69, 0.30)
	25%	3	405.4	0.38	0.50	720	4.21	(0.69, 0.29)

a) Turn-on voltage at 1 cd/m^2. b) Maximum luminance. c) Maximum current efficiency. d) Maximum power efficiency. e) Electroluminescence peaks. f) Maximum external quantum efficiency. g) Commission Internationale de L'Eclairage coordinates.

Reference

1 M.J. Frisch, G.W. Trucks, H.B. Schlegel, G.E. Scuseria, M.A. Robb, J.R. Cheeseman, G. Scalmani, V. Barone, G.A. Petersson, H. Nakatsuji, et al. Gaussian 16, Revision A.03, Gaussian, Inc.: Wallingford, CT, 2016.

2 Y. Yuan, J.-L. Liao, S.-F. Ni, A. K.-Y. Jen, C.-S. Lee, Y. Chi, *Adv. Funct. Mater.*, **2020**, *30*, 1906738.